Fracture Mechanics of Concrete and Concrete Structures -
Assessment, Durability, Monitoring and Retrofitting of Concrete Structures- B. H. Oh, et al. (eds)

An analytical model for FRP-concrete debonding based on an exponential softening law

P. Cornetti & Al. Carpinteri
Politecnico di Torino, Torino, Italy

ABSTRACT: Among rehabilitation strategies, bonding of Fiber Reinforced Polymers (FRP) sheets/plates is becoming more and more popular, especially for what concerns concrete structures. The performance of the interface between FRP and concrete is one of the key factors affecting the behavior of the strengthened structure. Up to now, closed-form analytical solutions exist only for the local bond-slip law with linear softening. Aim of the present paper is to show that analytical solutions can be achieved also assuming an exponential decaying softening law. Accordingly, the expressions for the interfacial shear stress distribution and the load-displacement response are derived for the different loading stages. A full parametric analysis of the problem has been performed, highlighting the size effect on the structural behavior as well as the effects of the bond length, of the FRP stiffness and of the interface constitutive law. A comparison with other analytical models available in the literature concludes the paper.

1 INTRODUCTION

Bonding of FRP has emerged as a wide-spread method for retrofitting existing concrete structures. In this technique, the performance of the FRP-to-concrete interface is of primary importance. The failure mode of FRP-reinforced beams is often directly related to the debonding of the FRP plate from the substrate. The debonding of the plate may take place either from the edge of the FRP strip or from an intermediate flexural crack. The former failure mode is named edge debonding, whereas the latter is usually referred to as intermediate crack induced debonding (IC-debonding) (Carpinteri et al. 2009a).

In IC-debonding failure, the stress state is similar to that of a push-pull shear test (Fig. 1), where a plate is bonded to a concrete block and is subjected to tension. It is a kind of single lap joint. Because of its (relative) simplicity, several experiments as well as theoretical analyses have been concerned with such a test geometry. Experiments show that, in such joints, the principal failure mode is concrete failure under shear, leading to a main crack running few millimeters beneath the concrete-to-adhesive interface. Thus, the maximum transferable load of the joint strongly depends on concrete mechanical properties.

Several works are available in the literature about the pull-push shear test (see, e.g., Wu et al. 2002, Yuan et al. 2004, Leung & Yang 2006, and references herein). However, an analytical solution for the complete debonding process of the joint is available in closed-form only for a local bond-slip law with linear softening, sometimes referred to as bi-linear law (Yuan et al. 2004). Aim of the present paper is to provide an analytical solution for an exponentially decaying softening of the interfacial stress-displacement law. Up to now, the solution of such a problem has been achieved only numerically (see, e.g., Ferracuti et al. 2006). Finally observe that, although attention is focused on FRP-to-concrete bonded joints, the present analysis is applicable also to other kind of reinforcements, e.g. steel plates.

2 GOVERNING EQUATIONS

Figure 1 shows a single-lap pull-push test of a plate-to-concrete bonded joint, in which the width and thickness of each of the three components (plate, adhesive layer and concrete prism) are constant along the length. The width and thickness of the reinforcement plate are denoted respectively by t_r and h_r, those of the concrete prism by t_b and h_b, and the bonded length of plate is denoted by l; x is the longitudinal coordinate. The Young's moduli of plate and concrete are E_r and E_b respectively. In such a joint, the adhesive layer is mainly subjected to shear deformations, so that mode II interfacial fracture is the expected failure mode. Note that a rigorous elastic analysis of the problem show that also a mode I component (i.e. peeling stresses) is present (Suo & Hutchinson 1990), but we will neglect such a contribution. A simple mechanical model for this joint can thus be established by treating the plate and the concrete prism (the two adherents) as being subject to axial deformations only, while the adhesive layer

can be assumed to be subject to shear deformations only. That is, both adherents are assumed to be subject to uniformly distributed axial stresses, with any bending effects neglected, while the adhesive layer is assumed to be subject to shear stresses which are also constant across the thickness of the adhesive layer. It should be noted that, in such a model, the adhesive layer represents not only the deformation of the actual adhesive layer, but also that of the materials adjacent to the adhesive. Based on these assumptions, the equilibrium equations of the reinforcement and of the overall joint read respectively:

$$h_r \frac{d\sigma_r}{dx} - \tau = 0 \quad (1)$$

$$\sigma_r h_r t_r + \sigma_b h_b t_b = 0 \quad (2)$$

where τ is the shear stress in the adhesive layer, σ_r is the axial stress in the reinforcement plate and σ_b is the axial stress in the concrete prism. The constitutive equations for the adhesive layer and the two adherents are:

$$\tau = \tau(\delta) \quad (3)$$

$$\sigma_r = E_r \frac{du_r}{dx} \quad (4)$$

$$\sigma_b = E_b \frac{du_b}{dx} \quad (5)$$

where u_r and u_b are the longitudinal displacements of the reinforcement and of the concrete, respectively. By means of Equations (1-5), it is possible to achieve the following second order differential equation in the interfacial slip δ, defined as the relative displacement between the two adherents (i.e. $\delta = u_r - u_b$):

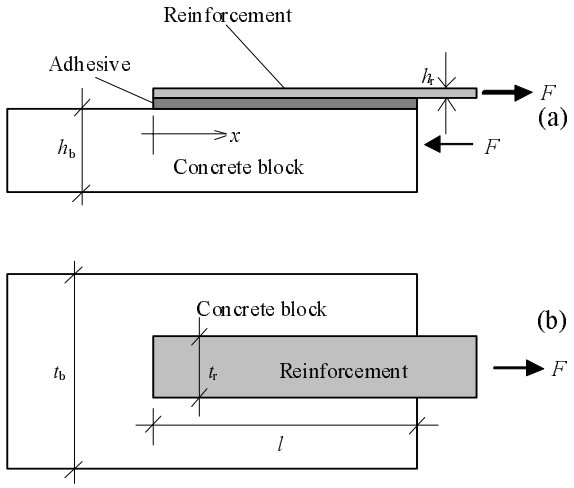

Figure 1. Pull-push shear test of a single lap bonded joint: (a) elevation; (b) plan.

$$\frac{d^2\delta}{dx^2} - \frac{1+\rho}{E_r h_r}\tau(\delta) = 0 \quad (6)$$

where ρ is the mechanical fraction of reinforcement (i.e. $\rho = E_r t_r h_r / E_b t_b h_b$). Observe that, by Equation (2) and by definition of slip, it is possible to express the stress in the FRP as a function of the first derivative of the slip:

$$\sigma_r = \frac{E_r}{1+\rho}\frac{d\delta}{dx} \quad (7)$$

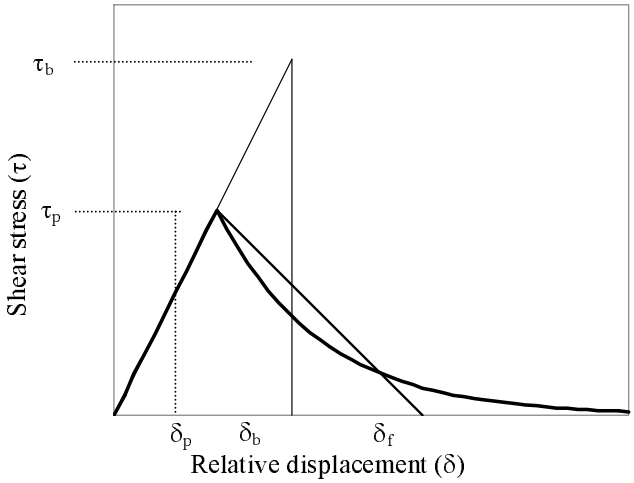

Figure 2. Local bond-slip model: elastic-perfectly brittle model (thin line); bi-linear model (medium line); elastic-exponential softening model (thick line). The models are compared with the same elastic slope and fracture energy (i.e. the same area beneath each curve).

3 COHESIVE LAW OF THE INTERFACE

In Yuan et al. 2004, an analytical solution based on a linear softening bond-slip law was presented. However, this kind of law is often not realistic; furthermore, as it will be shown later, its use can lead to overestimate the mechanical properties of the joint. Among the different interfacial laws available in the literature, we will use the one (Fig. 2) recently proposed by Neale et al. 2006 (on the basis of the analysis presented in Lu et al. 2005), characterized by a linear phase, with slope k, followed by an exponential softening branch. Let us denote by τ_p and δ_p the peak shear stress and the related slip, respectively ($k = \tau_p/\delta_p$). Introducing the dimensionless relative displacement $y = \delta/\delta_p$, the interfacial cohesive law is expressed analytically as:

$$\frac{\tau}{\tau_p} = f(y) = \begin{cases} y, & \text{if } 0 \le y \le 1 \\ e^{-2\alpha^2(y-1)}, & \text{if } y \ge 1 \end{cases} \quad (8)$$

where α^2 is a (positive) coefficient characterizing the exponential decay. The area beneath the curve represents the interface mode II fracture energy $\mathcal{G}_{IIc}$:

$$\mathcal{G}_{IIc} = \int_0^\infty \tau(\delta)\mathrm{d}\delta = \frac{\tau_p \delta_p}{2}\left(1+\frac{1}{\alpha^2}\right) \tag{9}$$

From Equation (9) it is evident that α^2 represents the ratio between the area beneath the elastic line and the area beneath the softening branch. For $\alpha\to\infty$, the cohesive law (8) represents an elastic-perfectly brittle interface, whereas for $\alpha\to 0$, it represents an elastic perfectly-plastic interface.

4 ANALYSIS OF THE DEBONDING PROCESS

In order to solve Equation (6), it is more convenient to use a dimensionless formulation. The longitudinal coordinate is normalized with respect to the bond length l, i.e. $\xi = x/l$. Hence, in Equation (6), δ and x may be replaced respectively by y and ξ, yielding:

$$\frac{\mathrm{d}^2 y}{\mathrm{d}\xi^2} - \beta^2 f(y) = 0 \tag{10}$$

where $y(\xi)$ is the unknown function and:

$$\beta = l\sqrt{\frac{1+\rho}{E_r h_r}\frac{\tau_p}{\delta_p}} \tag{11}$$

Before starting to analyze the different stages of the debonding process, it is worth recalling that, for a given set of material and geometrical parameters, the failure load is a monotonically increasing function of the bond length l. However, for a bond length tending to infinity, it can be proved that the failure load tends to the following asymptotic value:

$$F_c^\infty = t_r\sqrt{\frac{2\mathcal{G}_{IIc}E_r h_r}{1+\rho}} \tag{12}$$

In other words, F_c^∞ represents the maximum force that the joint can transfer. Interestingly, it depends only on the fracture energy, i.e. it does not depend on the shape of the interfacial cohesive law. Observe that this behavior is peculiar of external reinforcements. In fact, for internal reinforcing bars, there is always an anchorage length above which the full tensile strength of the reinforcement can be exploited.

The single lap joint is characterized by the load vs. displacement curve. The displacement of the bonded joint is defined as the slip at the loaded end (i.e. the value of δ at $x=l$) and is denoted by Δ. Hence:

$$\frac{\Delta}{\delta_p} = y(1) \tag{13}$$

The force F at the loaded end of the reinforcement may be evaluated by means of Equation (7) as $F = t_r\, h_r\, \sigma_r(x=l)$. By normalizing the force with respect to the maximum transferable force (12) and through analytical manipulations, we get:

$$\frac{F}{F_c^\infty} = \frac{\alpha}{\beta\sqrt{1+\alpha^2}}y'(1) \tag{14}$$

Equations (13) and (14) define the parametric plot of the load vs. displacement curve.

4.1 *Elastic stage*

During the elastic stage, all the joint is in the elastic regime, i.e. $y<1$ for any ξ. We may prescribe that, at the loaded end, the dimensionless displacement $y(1)$ is equal to u, with $0<u<1$. According to linear elasticity, this setting is equivalent to impose that the shear stress at the loaded end divided by the peak stress, i.e. τ/τ_p, is equal to u. The second boundary condition states that the other extreme of the reinforcement is unloaded, i.e. $y'(0)=0$ because of Equation (7). In formulae:

$$\begin{cases} y'' - \beta^2 y = 0, & 0 \le \xi \le 1 \\ y'(0) = 0 & \\ y(1) = u, & 0 \le u \le 1 \end{cases} \tag{15}$$

The general solution of the (linear) differential equation reads:

$$y(\xi) = c_1 e^{\beta\xi} + c_2 e^{-\beta\xi} \tag{16}$$

The two arbitrary constants have to be determined by means of the boundary conditions. Hence:

$$y(\xi) = \frac{\cosh(\beta\xi)}{\cosh(\beta)}u = \frac{\tau(\xi)}{\tau_p} \tag{17}$$

$$y'(\xi) = \beta\frac{\sinh(\beta\xi)}{\cosh(\beta)}u \tag{18}$$

Because of the elastic regime, the relative displacement (17) represents also the shear stress. For $u = 0.5$ (and $\beta = 3$), the stress field is represented by curve A in Figure 3.

4.2 *Elastic-softening stage*

At the end of the elastic stage, the shear stress reaches its peak at the loaded end of the joint. Al-

though the structural behavior of the joint depends on the test control, we assume as the control parameter the position of the stress peak in order to obtain all the possible solutions satisfying the governing equation (10). In other words, we make the assumption that the stress peak travels from the loaded end to the unloaded extreme. Let us denote with $\bar{\xi}$ that position. It divides the bonded joint into two regions: the former ($0 \le \xi \le \bar{\xi}$) is in the elastic regime, the latter is in the softening regime ($\bar{\xi} \le \xi \le 1$). Since, at the peak, y is equal to unity, the differential problem governing the solution of the elastic zone is:

$$\begin{cases} y'' - \beta^2 y = 0, \quad 0 \le \xi \le \bar{\xi} < 1 \\ y'(0) = 0 \\ y(\bar{\xi}) = 1, \end{cases} \tag{19}$$

The general solution is still given by Equation (16). However, because of the different boundary conditions, the solution now reads:

$$y(\xi) = \frac{\cosh(\beta\xi)}{\cosh(\beta\bar{\xi})} = \frac{\tau(\xi)}{\tau_p} \tag{20}$$

$$y'(\xi) = \beta \frac{\sinh(\beta\xi)}{\cosh(\beta\bar{\xi})} \tag{21}$$

Between the point ($\xi=\bar{\xi}$) where the shear stress reaches its peak and the loaded end ($\xi=1$), the joint is in the softening regime: the differential equation changes accordingly and it is not linear any more. On the other hand, the boundary conditions are given by the continuity conditions (respectively for the relative displacement and the tensile force in the reinforcement) with the zone in the elastic regime and can therefore be obtained by evaluating Equations (20-21) at $\xi=\bar{\xi}$:

$$\begin{cases} y'' - \beta^2 e^{-2\alpha^2(y-1)} = 0, \quad 0 < \bar{\xi} \le \xi \le 1 \\ y(\bar{\xi}) = 1 \\ y'(\bar{\xi}) = \beta \tanh(\beta\bar{\xi}) \end{cases} \tag{22}$$

Analytical details about how to achieve the solution of the differential problem (22) will be given elsewhere. The final solution reads:

$$y(\xi) = 1 + \frac{1}{\alpha^2} \times \\ \times \ln \frac{\cosh[\alpha\beta\gamma(\xi - \bar{\xi}) + \ln(\gamma + \alpha \tanh(\beta\bar{\xi}))]}{\cosh[\ln(\gamma + \alpha \tanh(\beta\bar{\xi}))]} \tag{23}$$

$$y'(\xi) = \frac{\beta\gamma}{\alpha} \tanh\left[\alpha\beta\gamma(\xi - \bar{\xi}) + \ln\left(\gamma + \alpha \tanh(\beta\bar{\xi})\right)\right] \tag{24}$$

with $\gamma = [\alpha^2 \tanh^2(\beta\bar{\xi}) + 1]^{1/2}$. The stress field is then obtained upon substitution of Equation (23) into the constitutive law (8):

$$\frac{\tau(\xi)}{\tau_p} = \left\{ \frac{\cosh[\ln(\gamma + \alpha \tanh(\beta\bar{\xi}))]}{\cosh[\alpha\beta\gamma(\xi - \bar{\xi}) + \ln(\gamma + \alpha \tanh(\beta\bar{\xi}))]} \right\}^2 \tag{25}$$

For $\bar{\xi}$ = 0.5 (and α=0.7, β=3), the stress field given by Equations (20) and (25) is represented by curve B in Figure 3.

4.3 *Softening stage*

When the peak of the shear stress reaches the unloaded side of the FRP strip, all the joint is in the softening regime. The maximum shear stress is now fixed at ξ = 0; its value is assumed to decrease from τ_p to 0, the latter value corresponding to final failure. Therefore, the stress field in the softening regime can be obtained by imposing that the normalized shear stress, τ/τ_p, at the unloaded end is equal to the parameter v, with $0<v<1$. The boundary condition on the stress may be converted into a displacement condition by means of the constitutive law (8). The related differential problem reads:

$$\begin{cases} y'' - \beta^2 e^{-2\alpha^2(y-1)} = 0, \quad 0 \le \xi \le 1 \\ y(0) = 1 - \dfrac{\ln v}{2\alpha^2}, \quad 0 < v \le 1 \\ y'(0) = 0 \end{cases} \tag{26}$$

whose solution is:

$$y(\xi) = 1 + \frac{1}{\alpha^2} \ln \frac{\cosh(\alpha\beta\xi\sqrt{v})}{\sqrt{v}} \tag{27}$$

$$y'(\xi) = \frac{\beta\sqrt{v}}{\alpha} \tanh\left[\alpha\beta\xi\sqrt{v}\right] \tag{28}$$

The stress field is then obtained upon substitution of Equation (27) into the constitutive law (8):

$$\frac{\tau(\xi)}{\tau_p} = \frac{v}{\cosh^2(\alpha\beta\xi\sqrt{v})} \tag{29}$$

For v = 0.5 (and α=0.7, β=3), the stress field is represented by curve C in Figure 3.

4.4 *Load vs. displacement curve*

Upon evaluation of Equations (17-18), (23-24) and (27-28) at ξ=1, and by means of Equations (13-14), it is possible to achieve the load F vs. displacement Δ characterizing the joint. It is interesting to point out

that the shape of the dimensionless plot, i.e. F/F_c^{∞} vs. $y(1)$, depends uniquely on the two dimensionless parameter α and β. The former is related to the parameters of the cohesive law by the following relationship:

$$\alpha = \left(\frac{2\mathcal{G}_{IIc}}{\tau_p \delta_p} - 1 \right)^{-1/2} \tag{30}$$

Which derives directly from Equation (9). The latter parameter is provided by Equation (11) and depends on the geometrical dimensions and on the stiffness of both the adherents and the adhesive. A typical load vs. displacement curve is plotted in Figure 4 (α=0.7 and β=3). The 01 line corresponds to the elastic regime; the 12 arc to the elastic-softening phase, where the maximum load is reached; the 23 branch is attained when all the joint is in softening condition. Note that the stress fields corresponding to points A,B,C in Figure 4 are the ones marked by the same letter in Figure 3.

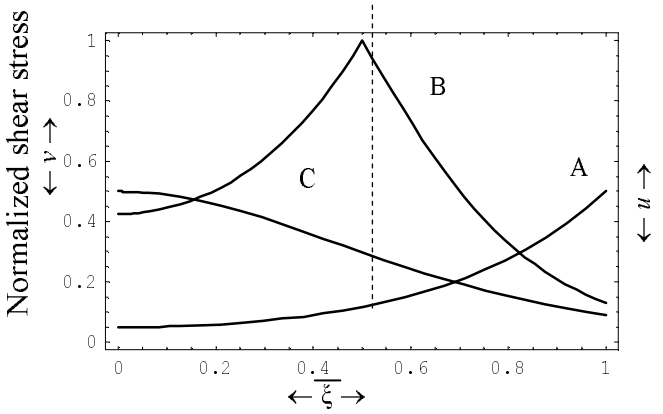

Figure 3. Interfacial shear stress distribution (α=0.7, β=3): elastic (A), elastic-softening (B) and softening (C) stage. ξ=0 corresponds to the unloaded end and ξ=1 corresponds to the loaded end.

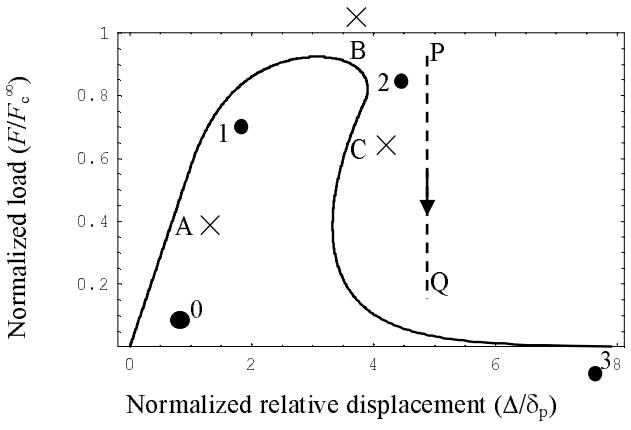

Figure 4. Typical full-range load-displacement curve (α=0.7, β=3): the line 01 corresponds to the elastic stage, the arc 12 to the elastic-softening stage and the branch 23 to the softening phase. The stress field corresponding to point A,B,C are represented by the curves A,B,C in Figure 3. The dashed line PQ represents the snap-back occurring if the test is displacement-controlled.

Note that, in the case considered in Figure 4, the application of the simple stress criterion $\tau=\tau_p$ would have provided a failure load (point 1) approximately equal to 2/3 of the actual one (point B). This means that the maximum shear stress may be attained under service loading. On the other hand, the maximum load is achieved when about one half of the bond length is in the softening regime (curve B in Fig. 3). These considerations fully justify the nonlinear analysis herein proposed.

Finally, it is worth observing that, if the test is displacement-controlled, the displacement Δ is monotonically increasing during the test. It means that a snap-back instability (Carpinteri 1985, 1989) occurs, i.e. a sudden load drop at fixed displacement from point P to Q (dashed line in Fig. 4). On the other hand, if the test is load-controlled, after the peak load the interfacial crack propagates always unstably up to global failure, i.e. no snap-through may occur.

5 PARAMETRIC ANALYSIS

Taking as fundamental quantities the peak stress τ_p and the thickness of the FRP plate h_r, dimensional analysis shows that, during the debonding process, the dimensionless load and edge displacement depend on the following dimensionless ratios:

$$\left.\begin{matrix} \dfrac{F}{\tau_p h_r^2} \\ \dfrac{\Delta}{h_r} \end{matrix}\right\} = f\left(\frac{t_b}{h_r}; \frac{t_r}{h_r}; \frac{h_b}{h_r}; \frac{l}{h_r}; \frac{E_r}{\tau_p}; \frac{E_b}{\tau_p}; \alpha; \frac{\mathcal{G}_{IIc}}{\tau_p h_r} \right) \tag{31}$$

We define the last ratio, ruling the size effect, as the interface energetic brittleness number s_E:

$$s_E = \frac{\mathcal{G}_{IIc}}{\tau_p h_r} \tag{32}$$

This represents the extension to mode II debonding failure of the energetic brittleness number $\mathcal{G}_F/(\sigma_u h)$ introduced by Carpinteri (1981) for homogeneous quasi-brittle materials.

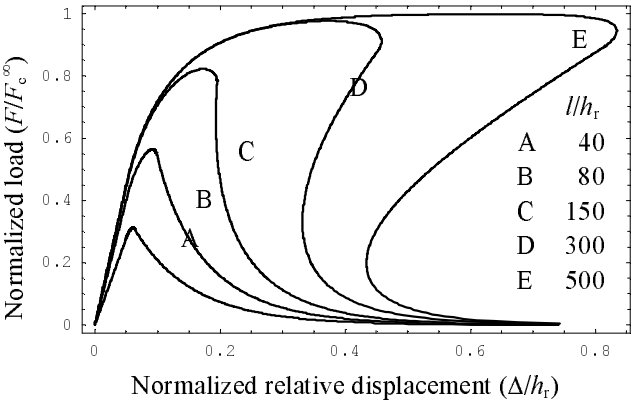

Figure 5. Effect of the bond length on load vs. displacement curve. Dimensionless ratios equal to h_b/h_r=100; t_r/h_r=25; t_b/h_r=100; E_r/τ_p=62,500; E_b/τ_p=7500; α=0.5; s_E=0.125.

5.1 *Effect of the bond length*

In Figure 5 we fixed all the parameters in Equation (31) except the ratio of the bond length l to the thickness of the FRP plate h_r. For the sake of clarity, the load is normalized with respect to F_c^∞ instead of $\tau_p h_r^2$. It is evident that, increasing the bond length, the elastic stiffness as well as the maximum load tend to a constant value. More in detail, the maximum transmissible force by the joint is F_c^∞, while the structural behaviour changes from quasi-brittle (curve A) to ductile-brittle (curve E). Note that, for relatively high bond lengths (curves C-D-E), a snap-back instability occurs. Finally, it is worth observing that, based on Figure 5, it is possible to define an effective bond length, i.e. a threshold length beyond which the maximum load is practically equal to F_c^∞.

5.2 *Effect of the FRP stiffness*

In Figure 6 we fixed all the parameters in Equation (31) except the ratio of the Young moduli of the FRP and of the concrete, i.e. E_r/E_b. Note that the same effect is obtained by varying h_r/h_b. It is seen that, increasing the reinforcement stiffness, the maximum load increases as well as the brittleness of the structural response. More in detail, the structural behaviour changes from quasi-brittle (curve A) to ductile-brittle (curve E). Note that, for relatively low FRP stiffnesses (curves C-D-E), the structural response is ductile up to a final snap-back instability. Eventually, it is worth observing that the area beneath each curve, which is proportional to the energy spent to have complete delamination, is constant and that, for high FRP stiffnesses, the effective bond length increases.

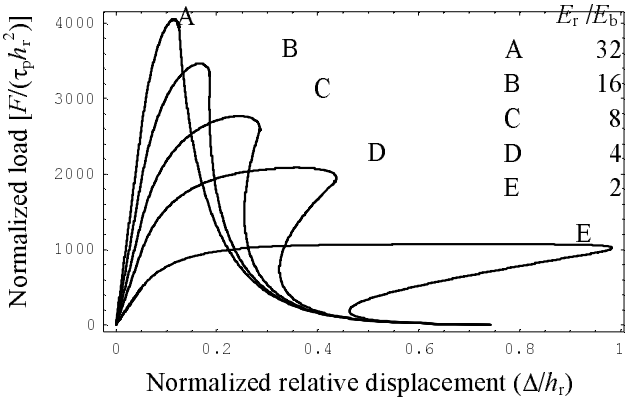

Figure 6. Effect of the FRP stiffness on load vs. displacement curve. Dimensionless ratios equal to h_b/h_r=100; t_r/h_r=25; t_b/h_r=100; l/h_r=200; E_b/τ_p=7500; α=0.5; s_E=0.125.

5.3 *Effect of the cohesive law*

We wish now to analyze the effect of the shape of the cohesive law, within the assumption of a linear ascending branch followed by an exponential tail (Eq. (8)). We consider two cases. In the former one, we keep τ_p and δ_p constant and let α vary (and s_E accordingly), see Figure 7a. All the other dimensionless ratios (Eq. (31)) are kept constant. Although τ_p is the same for all the curves, from Figure 7b it is evident that the presence of a softening branch gives rise to a strength supply beyond the elastic regime. In fact, the load at which the stress reaches τ_p at the loaded end is also the maximum load only for an elastic-perfectly brittle interface (curve A). On the other hand, the softening of the interface cohesive law makes the maximum load higher (curves B-C-D) and an horizontal plateau is reached for an elastic-perfectly plastic interface (curve E). Eventually, observe that a snap-back instability occurs only for strongly decaying softening branches, i.e. for relatively high α values (curves A-B-C).

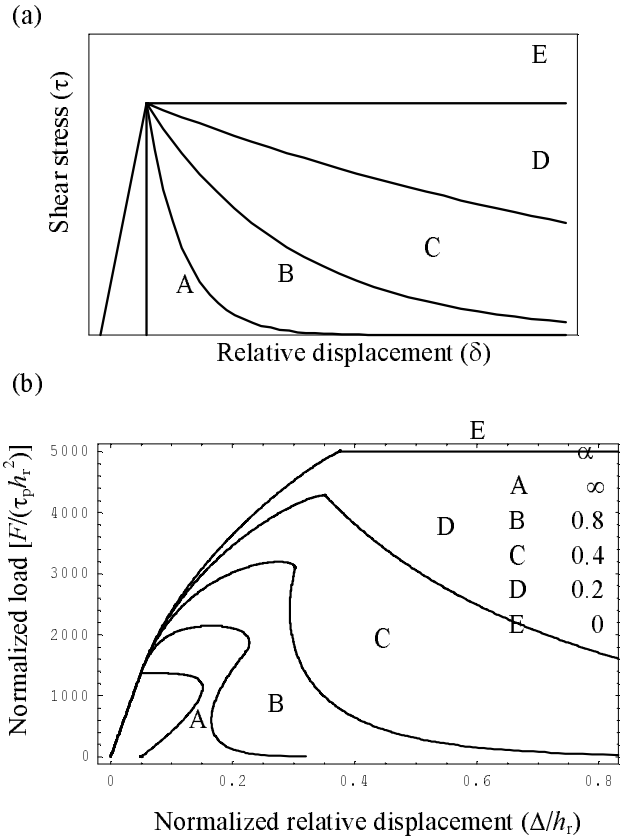

Figure 7. Effect of the interface law (a) on load vs. displacement curve (b) by varying α and keeping τ_p and δ_p constant. Dimensionless ratios equal to h_b/h_r=100; t_r/h_r=25; t_b/h_r=100; l/h_r=200; E_r/τ_p=62,500; E_b/τ_p=7500; $s_E=(1+\alpha^2)/(2\alpha^2)\times 5\times 10^{-2}$, i.e. δ_p/h_r= 0.05.

In the latter case, we keep $\mathcal{G}_{IIc}$ and k constant and let α vary (and s_E accordingly), see Figure 8a. All the other dimensionless ratios (Eq. (31)) are kept constant. Since now τ_p is varying, it is more convenient to normalize the load with respect to F_c^∞ instead of $\tau_p h_r^2$. Figure 8b shows that, for a given bond length, the maximum transmissible force F_c^∞ is attained only by the curves corresponding to rapidly decreasing softening branches. Note that, k being constant, the initial

(elastic) slope of the F-Δ curves is the same for all the curves; analogously, the area beneath each curve is constant since the energy required to have complete delamination is the same ($\mathcal{G}_{IIc} \times t_r \times l$). The snap-back instability disappears for very slowly decreasing softening branches (curve E), when the F-Δ curve early departs from the initial (elastic) straight line.

5.4 *Size effect*

In Figure 9 we fixed all the parameters in Equation (31) except the interface energetic brittleness number s_E. Varying s_E means, for instance, that the overall structural size changes while keeping constant all the geometrical ratios and material properties. Therefore, Figure 9 describes the size effect for the pull-push shear test. It shows that, increasing the interface energetic brittleness number, the structural behaviour changes from ductile-brittle to quasi-brittle and that the snap-back instability occurs for relatively low s_E values. It is important to highlight that brittleness is not a purely material property, but a structural one: in fact, low interface energetic brittleness numbers correspond to brittle interfaces and/or large sizes, while high s_E values correspond to ductile interfaces and/or relatively small sizes.

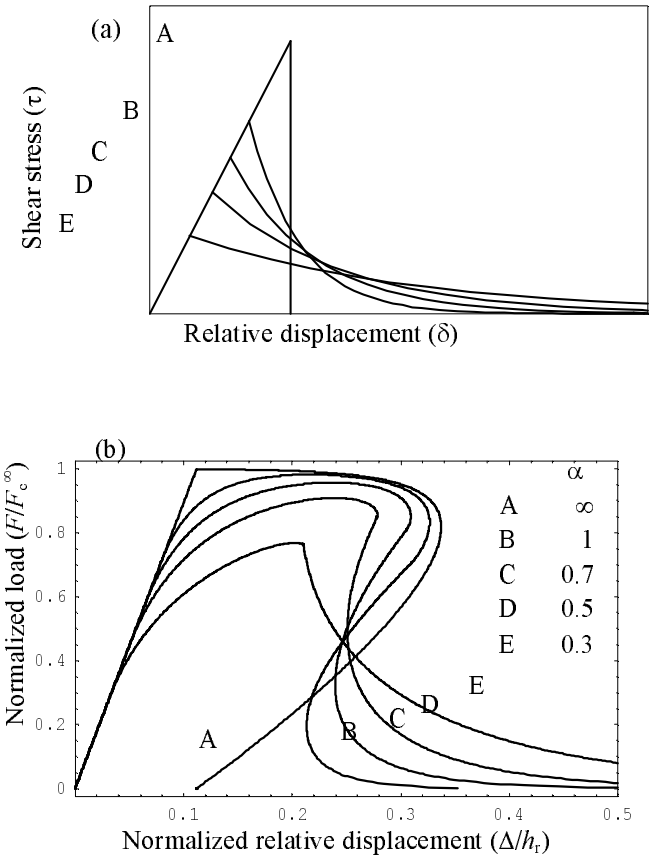

Figure 8. Effect of the interface law (a) on load vs. displacement curve (b) by varying α and keeping k and $\mathcal{G}_{IIc}$ fixed. Dimensionless ratios equal to h_b/h_r=100; t_r/h_r=25; t_b/h_r=100; l/h_r=200; $E_r h_r/\mathcal{G}_{IIc}$=5×10^5; $E_b h_r/\mathcal{G}_{IIc}$=6×10^4; s_E=[5(1+α^2)]$^{1/2}$/(40α), i.e. $k h_r^2/\mathcal{G}_{IIc}$=160.

5.5 *Interface laws: elastic-perfectly brittle, linear softening, exponential softening*

Fixing the geometrical aspect, in Figure 10 we compared the solutions provided by different cohesive laws, namely an elastic-perfectly brittle law, an elastic-linear softening law, and an elastic-exponentially softening law. We fixed the slope of the elastic branch and the fracture energy value, i.e. the area beneath the bond-slip law is constant for the three curves (Fig. 2). Therefore:

$$\delta_f = \frac{2\mathcal{G}_{IIc}}{\tau_p} \tag{33}$$

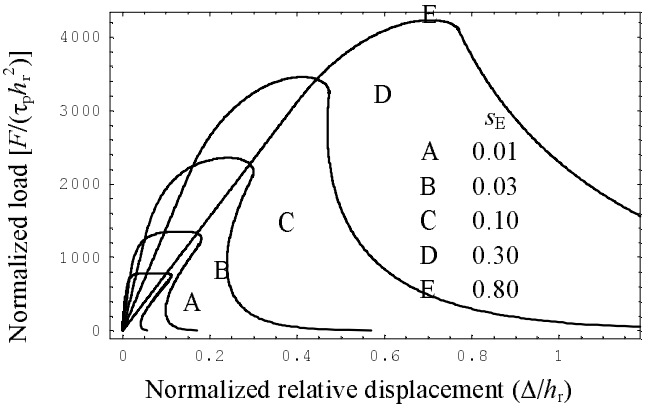

Figure 9. Size effect on load vs. displacement curve. Dimensionless ratios equal to h_b/h_r=100; t_r/h_r=25; t_b/h_r=100; l/h_r=200; E_r/τ_p=62,500; E_b/τ_p=7500; α=0.5.

$$\delta_b = \sqrt{\frac{2\mathcal{G}_{IIc}\delta_p}{\tau_p}}, \qquad \tau_b = \sqrt{\frac{2\mathcal{G}_{IIc}\tau_p}{\delta_p}} \tag{34}$$

For the meaning of the symbols, refer to Figure 2. For the curve corresponding to linear softening, the solution was taken from Yuan et al. 2004, whereas the curve corresponding to the elastic-perfectly brittle law derives directly from LEFM (Carpinteri et al 2009b). However, it is worth observing that the elastic-perfectly brittle case could be caught by the present model letting $\alpha \to \infty$.

In Figure 10 we plotted the results for two different joint lengths. The solution of the present model differs from the one corresponding to linear softening because of a stronger deviation from the initial slope of the ascending branch in the load vs. displacement curve. Furthermore, a residual – although small – transferable force is present also for large displacements because of the exponentially decaying shear stress.

A second aspect to be pointed out is that, while for sufficiently long joints the maximum transferable force is achieved for every interface law (Fig. 10b), for relatively short joints (Fig. 10a), F_c^∞ is reached only by the LEFM model. In other words, LEFM, as well as the linear softening model, tend to overesti-

mate the maximum transferable force of the joint with respect to the present model.

From a numerical point of view, it is worth noting that, although the linear softening looks more simple to handle than the exponential softening, the solution of the differential Equation is more complicated in the first case. This is due to the fact that, instead of the three stages (elastic, elastic-softening, softening), according to the linear softening the joint undergoes five different stages (elastic, elastic-softening, elastic-softening-debonding, softening-debonding, debonding). Furthermore, of these five stages, the third cannot be obtained in a fully analytical form since the equation relating the lengths of the softening and of the debonded zones has to be solved numerically.

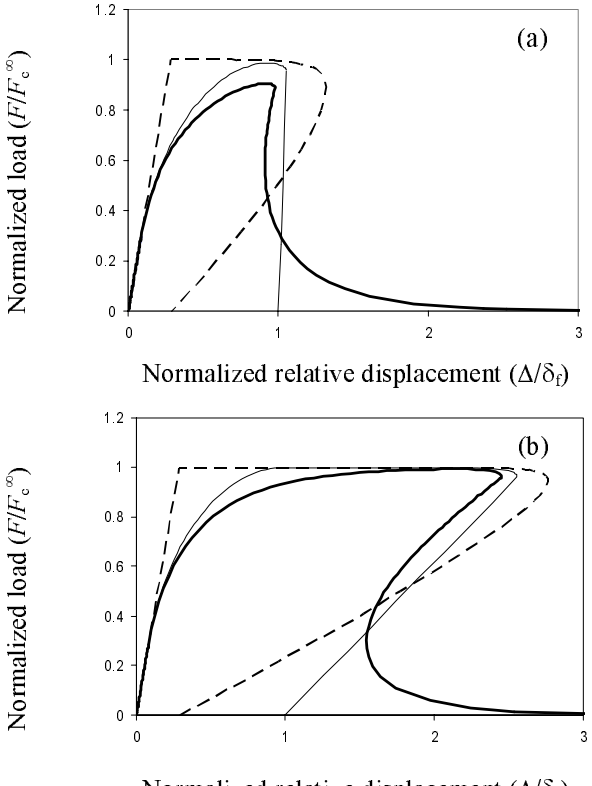

Figure 10. Load vs. displacement curve for different bond-slip model: elastic-perfectly brittle (dashed line), elastic-linear softening (thin line) and elastic-exponential softening (thick line). Values: h_r = 1.016 mm; h_b = 75 mm; t_r = 50 mm; t_b = 150 mm; E_b = 33,640 MPa; E_r = 230,000 MPa; τ_p = 6.64 MPa; δ_p = 0.039 mm; G_{IIc}= 1.59 N/mm. Figure (a) refer to a joint whose length is l = 200 mm; figure (b) to l = 400 mm.

6 CONCLUSIONS

In the present paper a closed-form solution describing the full-range behaviour of FRP-to-concrete bonded joints is presented. Restricting the analysis to the pull-push geometry, a dimensional and parametrical analysis of the problem has been performed, highlighting the effects on the solution of the bond length, the FRP stiffness, and the interface law. Moreover, also the size effect for the problem considered has been addressed.

Concerning the comparison with different models available in the literature, it is worth observing that: (*i*) models neglecting the interface nonlinearity (i.e. elastic-perfectly brittle interface law) usually provide very rough predictions; (*ii*) with respect to linear softening models, the present model is easier to be implemented (only 3 stages instead of 5) and it is believed to be more realistic; (*iii*) with respect to more sophisticated local bond-slip models (such as Ferracuti et al. 2006), the present approach provides similar results without a proper numerical analysis. Of course, the present analysis is restricted to a specific geometry (i.e. the pull-push test), but the approach is general: the solution procedure outlined can be easily extended to deal with similar test setups, such as the pull-pull shear test. These extensions, as well as the comparison with other analytical models for FRP debonding such as the three-parameter model by Leung & Tung 2006, will be the matter of future developments.

REFERENCES

Carpinteri, A. 1981. Static and energetic fracture parameters for rocks and concrete. *Material & Structures* 14: 151-162.

Carpinteri, A. 1985. Interpretation of the Griffith instability as a bifurcation of the global equilibrium. In Surendra P. Shah (ed.), *Application of fracture mechanics to cementitious composites:* 287-316. Dordrecht: Martinus Nijhoff Publishers.

Carpinteri, A. 1989. Cusp catastrophe interpretation of fracture instability. *Journal of the Mechanics and Physics of Solids* 37: 567-582.

Carpinteri, A., Cornetti, P., Lacidogna, G. and Paggi, M. 2009a. Towards a unified approach for the analysis of failure modes in FRP-retrofitted concrete beams. *Advances in Structural Engineering* 12(5): 715-729.

Carpinteri, A., Cornetti, P. and Pugno, N. 2009b. Edge debonding in FRP strengthened beams: Stress versus energy failure criteria. *Engineering Structures* 31: 2436-2447.

Ferracuti, B., Savoia, M. and Mazzotti, C. 2006. A numerical model for FRP-concrete delamination. *Composites Part B: Engineering* 37: 356-364.

Leung, C.K.Y. and Tung, W.K. 2006. Three-parameter model for debonding of FRP plate from concrete substrate. *Journal of Engineering Mechanics-ASCE* 132: 509-518.

Leung, C.K.Y. and Yang, Y. 2006. Energy-based modelling approach for debonding of FRP plate from concrete substrate. *Journal of Engineering Mechanics-ASCE* 132: 583-593.

Lu, X.Z., Teng, J.G., Ye, L.P. and Jiang, J.J. 2005. Bond-slip models for FRP sheets / plates bonded to concrete. *Engineering Structures* 27: 920-937.

Neale, K.W., Ebead, U.A., Abdel Baky, H.M., Elsayed, W.E. and Godat, A. 2006. Analysis of the load-deformation behaviour and debonding for FRP-strengthened concrete structures. *Advances in Structural Engineering* 9: 751-763.

Suo, Z. and Hutchinson, J.W. 1990. Interface crack between two elastic layers. *International Journal of Fracture* 43: 1-18.

Wu, Z., Yuan, H. and Niu, H. 2002. Stress transfer and fracture propagation in different kinds of adhesive joints. *Journal of Engineering Mechanics-ASCE* 128: 562-73.

Yuan, H., Teng, J.G., Seracino, R., Wu, Z.S. and Yao, J. 2004. Full-range behaviour of FRP-to-concrete bonded joints. *Engineering Structures* 26: 553-565.